J|A|C|S
ARTICLES
Published on Web 09/22/2006

Octahedral Non-Heme Oxo and Non-Oxo Fe(IV) Complexes: An Experimental/Theoretical Comparison

John F. Berry,† Eckhard Bill, Eberhard Bothe, Frank Neese,‡ and Karl Wieghardt*

Contribution from the Max-Planck-Institut für Bioanorganische Chemie, Stiftstrasse 34-36, D-45470 Mülheim an der Ruhr, Germany

Received May 23, 2006; E-mail: wieghardt@mpi-muelheim.mpg.de

Abstract: Electron-transfer series are described for three ferric complexes of the pentadentate ligand 4,8,11-trimethyl-1,4,8,11-tetraazacyclotetradecane-1-acetate (Me_3cyclam−acetate) with axial chloride, fluoride, and azide ligands. These complexes can all be reduced coulometrically to their Fe(II) analogs and oxidized reversibly to the corresponding Fe(IV) species. The Fe(II), Fe(III), and Fe(IV) species have been studied spectroscopically and their UV−vis, Mössbauer, EPR, and IR spectra are presented. The fluoro species $[(Me_3cyclam-acetate)FeF]^{n+}$ ($n = 0, 1, 2$) have been studied computationally using density functional theory (DFT), and the electronic structure of the Fe(IV) dication $[(Me_3cyclam-acetate)FeF]^{2+}$ is compared with that of the isoelectronic Fe(IV) oxo cation $[(Me_3cyclam-acetate)FeO]^{+}$; the different properties of the two species are mainly due to the significantly covalent Fe=O π bonds in the latter.

Introduction

Iron is the most prominent transition metal in biological systems and is known to play an active role in the catalytic cycles of many metalloenzymes.[1] By far, the most common oxidation states of iron in proteins are the +2 and +3 states, though higher oxidation states (+4 and +5) are often proposed for specific intermediates in oxygen-activating enzymes and model systems.[2−5] Because of these proposals, the chemistry of heme and non-heme iron in its high valent states is currently of intense interest, and synthetic routes to stable forms of these species have been sought.

A problem encountered in the chemistry of heme complexes in their higher oxidation states is that the porphyrin ligand itself can also be oxidized forming a π radical. In fact, in the class of oxidizing enzymes known as cytochromes P450, intermediates known as "Compound I" are believed to be the most active species in the catalytic cycle ultimately responsible for the hydroxylation of C−H bonds in substrates and are also believed to contain an Fe(IV)-oxo unit coordinated to an oxidized porphyrin radical.[6] In such species, the oxidation state of the iron would actually be higher if it were not for the oxidation of the porphyrin. Similar considerations have led to ambiguity in highly oxidized corrolate complexes, some of which have been claimed as examples of Fe(IV) complexes,[7] but corroleate ligands are also fairly easily oxidized,[8] and it is believed that these complexes are, in fact, Fe(III) complexes of corrolate radicals.[9,10]

In non-heme iron systems, the ligands bound to iron are generally considered to be redox-innocent, and intermediates containing Fe(IV) or Fe(V) have been postulated, and a high-spin Fe(IV)-oxo intermediate has been observed and studied spectroscopically in the case of the enzyme taurine/α-ketoglutarate dioxygenase.[11] In addition to work done by other groups in the synthesis and characterization of Fe(IV) complexes,[12−17] our laboratory has produced evidence for mono-[18] and dinuclear[19] Fe(IV) complexes, Fe(V) complexes,[18,20] and recently even Fe(VI) species.[21] For the mononuclear complexes, we have

† Current address: Department of Chemistry, University of Wisconsin−Madison, 1101 University Avenue, Madison, WI 53706.

‡ Current address: Institut für Physicalische und Theoretische Chemie, Universität Bonn, D-53115 Bonn, Germany.

(1) Lippard, S. J.; Berg, J. M. *Principles of Bioinorganic Chemistry*; University Science Books: Mill Valley, CA, 1994.
(2) Merkx, M.; Kopp, D. A.; Sazinsky, M. H.; Blazyk, J. L.; Muller, J.; Lippard, S. J. *Angew. Chem., Int. Ed.* **2001**, *40*, 2782.
(3) Costas, M.; Mehn, M. P.; Jensen, M. P.; Que, L., Jr. *Chem. Rev.* **2004**, *104*, 939.
(4) Bassan, A.; Blomberg, M. R. A.; Siegbahn, P. E. M.; Que, L., Jr. *Angew. Chem., Int. Ed.* **2005**, *44*, 2939.
(5) See the following special issue dedicated to Fe(IV) chemistry: Ghosh, A. *J. Inorg. Biochem.* **2006**, *100*, 419.
(6) Sono, M.; Roach, M. P.; Coulter, E. D.; Dawson, J. H. *Chem. Rev.* **1996**, *96*, 2841.
(7) Simkhovich, L.; Goldberg, I.; Gross, Z. *Inorg. Chem.* **2002**, *41*, 5433.
(8) Shen, J.; Shao, J.; Ou, Z.; E, W.; Koszarna, B.; Gryko, D. T.; Kadish, K. M. *Inorg. Chem.* **2006**, *45*, 2251.
(9) Nardis, S.; Paolesse, R.; Licoccia, S.; Fronczek, F. R.; Vicente, M. G. H.; Shokhireva, T. K.; Cai, S.; Walker, F. A. *Inorg. Chem.* **2005**, *44*, 7030.
(10) Walker, F. A.; Licoccia, S.; Paolesse, R. *J. Inorg. Biochem.* **2006**, *100*, 810.
(11) Price, J. C.; Barr, E. W.; Tirupati, B.; Bollinger, J. M.; Krebs, C. *Biochemistry* **2003**, *42*, 7497.
(12) Betley, T. A.; Peters, J. C. *J. Am. Chem. Soc.* **2004**, *126*, 6252.
(13) Cummins, C. C.; Schrock, R. R. *Inorg. Chem.* **1994**, *33*, 395.
(14) Chanda, A.; Popescu, D.-L.; de Oliveira, F. T.; Bominaar, E. L.; Ryabov, A. D.; Münck, E.; Collins, T. J. *J. Inorg. Biochem.* **2006**, *100*, 606.
(15) Jensen, M. P.; Costas, M.; Ho, R. Y. N.; Kaizer, J.; Payeras, A. M. I.; Münck, E.; Que, L., Jr.; Rohde, J. U.; Stubna, A. *J. Am. Chem. Soc.* **2005**, *127*, 10512.
(16) Pestovsky, O.; Stoian, S.; Bominaar, E. L.; Shan, X. P.; Münck, E.; Que, L., Jr.; Bakac, A. *Angew. Chem., Int. Ed.* **2005**, *44*, 6871.
(17) Pestovsky, O.; Stoian, S.; Bominaar, E. L.; Shan, X.; Münck, E.; Que, L., Jr.; Bakac, A. *Angew. Chem., Int. Ed.* **2006**, *45*, 340.
(18) Grapperhaus, C. A.; Mienert, B.; Bill, E.; Weyhermüller, T.; Wieghardt, K. *Inorg. Chem.* **2000**, *39*, 5306.
(19) Slep, L. D.; Mijovilovich, A.; Meyer-Klaucke, W.; Weyhermüller, T.; Bill, E.; Bothe, E.; Neese, F.; Wieghardt, K. *J. Am. Chem. Soc.* **2003**, *125*, 15554.
(20) Meyer, K.; Bill, E.; Mienert, B.; Weyhermüller, T.; Wieghardt, K. *J. Am. Chem. Soc.* **1999**, *121*, 4859.
(21) Berry, J. F.; Bill, E.; Bothe, E.; George, S. D.; Mienert, B.; Neese, F.; Wieghardt, K. *Science* **2006**, *312*, 1937.

Scheme 1

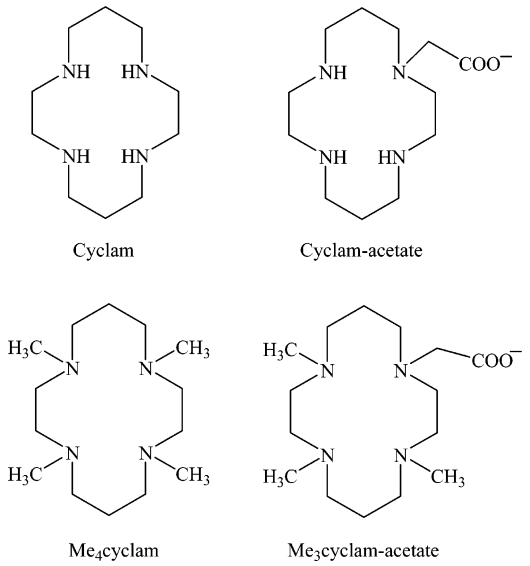

utilized the supporting tetradentate ligand cyclam (see Scheme 1) because of its properties as a spectroscopically and redox-innocent ligand, which can coordinate iron with four equatorial nitrogen donors akin to the coordination mode of a porphyrin ligand.

A high-valent Fe(V)-nitrido species formulated as [(cyclam)-$FeN(N_3)$]ClO_4 was characterized by our group,[20] as well as a similar Fe(V)-nitrido complex [(cyclam−acetate)$FeN]PF_6$ having the modified cyclam−acetate ligand,[18] which has been characterized in more detail than the former complex. In particular, it should be noted that the original reports of [(cyclam)$FeN(N_3)$]ClO_4 and [(cyclam−acetate)$FeN]PF_6$ had claimed both of the complexes to be high spin ($S = {}^3/_2$), whereas further study of the latter complex has conclusively shown it to be low-spin with a nearly orbitally degenerate doublet ground state.[22] Using the cyclam−acetate ligand, we also reported that the complex [(cyclam−acetate)Fe(OTf)]PF_6 reacts with ozone to produce a very reactive green species which was formulated as an Fe(IV)-oxo species ([(cyclam−acetate)FeO]PF_6) based on its Mössbauer spectrum.[18] After this work, the group of Que reported that the corresponding Fe(IV)-oxo complex of the ligand Me_4cyclam ([(Me_4cyclam)$FeO(NCCH_3)$]$(OTf)_2$) was stable enough that it could be crystallized and its crystal structure has been obtained.[23]

Because the addition of methyl groups to the cyclam ligand has been shown to be an effective method of stabilizing high valent iron species, the addition of methyl groups to the cyclam−acetate ligand so as to produce Me_3cyclam−acetate is a logical extension of our previous work in this area with the original aim of further stabilizing Fe(IV) and Fe(V) species. In using the Me_3cyclam−acetate ligand, three surprising discoveries were made. First, the Fe(III) complexes of Me_3cyclam−acetate were found to be high spin (whereas trans complexes of cyclam−acetate and cyclam itself are always low spin).[24] Second, octahedral Fe(III) complexes of Me_3cyclam−acetate can be reversibly oxidized to their corresponding Fe(IV) species (such oxidations are irreversible for cyclam−acetate complexes).[24] Third, the mononuclear azido−Fe(IV) complex [(Me_3-cyclam−acetate)FeN_3]$(PF_6)_2$ (hereafter designated **3ox**) has been found to be photoactive producing the diamagnetic nitrido−Fe(VI) species [(Me_3cyclam−acetate)$Fe^{VI}N]^{2+}$ upon irradiation with 650 nm light in acetonitrile solution.[21] Thus, the coordination chemistry of the Me_3cyclam−acetate ligand with iron extends access to high-valent Fe(IV) → Fe(VI).

In studying the first observation, an understanding of the effects (mainly steric and electronic effects) responsible for the spin state of ferric compounds of these ligands has been reached,[25] owing in large part to the work done by the Meyerstein group[26] on alkylated and nonalkylated macrocyclic ligands and their complexes. The second observation allows us to gain unique insights into the nature of iron in its tetravalent state as the ligand field is changed in a controlled manner. This is possible by studying [(Me_3cyclam−acetate)$FeX]^{2+}$ species with various X anions ($X{=}Cl^-$, N_3^-, F^-), which is the basis of the experimental part of this report. The effect of a terminal oxo ligand on the electronic structure is also probed in this report theoretically by comparing [(Me_3cyclam−acetate)$FeF]^{2+}$ with the isoelectronic [(Me_3cyclam−acetate)$FeO]^+$ species, which is similar to [(cyclam−acetate)$FeO]^{2+}$ [18] and the handful of Fe(IV)-oxo complexes which have been characterized in the Que lab.[15−17,23,27−31] Finally, the third observation has enabled the preparation and spectroscopic characterization of the second Fe(VI) complex yet to be prepared.[21]

Results and Discussion

Synthesis. The oxo-bridged diiron(III) species (Me_3cyclam−acetate)Fe−O−$FeCl_3$ is a convenient starting material for the synthesis of other complexes of the Me_3cyclam−acetate ligand. As shown in Scheme 2, the −(μ-O)$FeCl_3$ moiety is easily hydrolyzed and removed as rust and the axial ligand can be replaced by chloride, fluoride, or azide. Interestingly, if the hydrolysis is performed in a concentrated solution of KPF_6, precipitation of the bright-yellow chloro complex [(Me_3cyclam−acetate)FeCl]PF_6, **1**, occurs, whereas if a dilute solution of KPF_6 is used, only rust precipitates and if the resulting yellow filtrate is allowed to stand, crystals of the brilliant-yellow fluoro complex [(Me_3cyclam−acetate)FeF]PF_6, **2**, form over the course of several days (this time allows the slow acid-catalyzed hydrolysis of the PF_6 anions to occur). It was subsequently found that **2** can be formed in much better yields and purity by heating an aqueous solution of **1** in air, which accelerates the hydrolysis of the PF_6 anions. After a few minutes of heating, a rusty brown precipitate appears in the flask, and the resulting filtrate is brilliant-yellow in color and yields crystals of **2** upon standing. Using a concentrated solution of KPF_6 and NaN_3, the azido

(22) Aliaga-Alcalde, N.; George, S. D.; Mienert, B.; Bill, E.; Wieghardt, K.; Neese, F. *Angew. Chem., Int. Ed.* **2005**, *44*, 2908.
(23) Rohde, J. U.; In, J. H.; Lim, M. H.; Brennessel, W. W.; Bukowski, M. R.; Stubna, A.; Münck, E.; Nam, W.; Que, L., Jr. *Science* **2003**, *299*, 1037.
(24) Berry, J. F.; Bill, E.; Bothe, E.; Weyhermüller, T.; Wieghardt, K. *J. Am. Chem. Soc.* **2005**, *127*, 11550.
(25) Berry, J. F.; Bill, E.; Garcia-Serres, R.; Neese, F.; Weyhermüller, T.; Wieghardt, K. *Inorg. Chem.* **2006**, *45*, 2027.
(26) Meyerstein, D. *Coord. Chem. Rev.* **1999**, *186*, 141.
(27) Lim, M. H.; Rohde, J. U.; Stubna, A.; Bukowski, M. R.; Costas, M.; Ho, R. Y. N.; Münck, E.; Nam, W.; Que, L., Jr. *Proc. Natl. Acad. Sci. U.S.A.* **2003**, *100*, 3665.
(28) Bukowski, M. R.; Koehntop, K. D.; Stubna, A.; Bominaar, E. L.; Halfen, J. A.; Münck, E.; Nam, W.; Que, L., Jr. *Science* **2005**, *310*, 1000.
(29) Sastri, C. V.; Park, M. J.; Ohta, T.; Jackson, T. A.; Stubna, A.; Seo, M. S.; Lee, J.; Kim, J.; Kitagawa, T.; Münck, E.; Que, L., Jr.; Nam, W. *J. Am. Chem. Soc.* **2005**, *127*, 12494.
(30) Klinker, E. J.; Kaizer, J.; Brennessel, W. W.; Woodrum, N. L.; Cramer, C. J.; Que, L., Jr. *Angew. Chem., Int. Ed.* **2005**, *44*, 3690.
(31) Rohde, J. U.; Que, L., Jr. *Angew. Chem., Int. Ed.* **2005**, *44*, 2255.

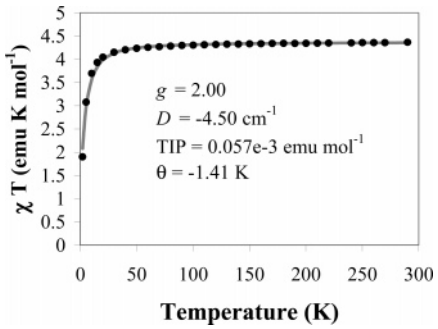

Figure 1. Magnetic susceptibility data for **1** from 2 to 300 K, which have been corrected for intrinsic diamagnetism as well as temperature-independent paramagnetism (TIP). The solid line represents a least-squares fit of the data based on a spin Hamiltonian simulation. (Inset) Fitting parameters.

Scheme 2

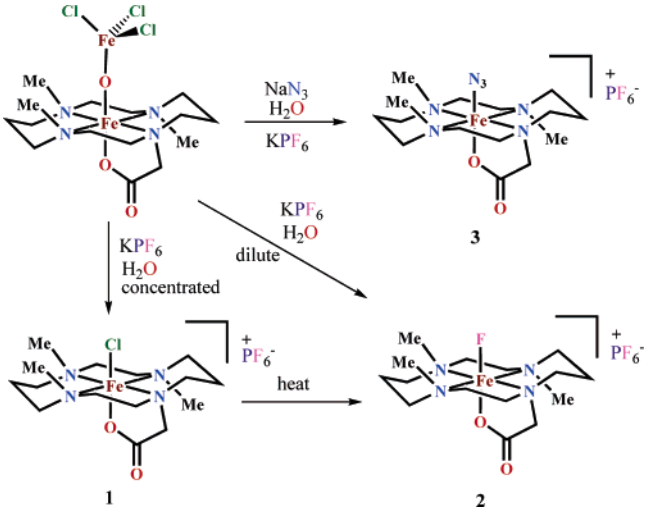

complex [(Me$_3$cyclam−acetate)FeN$_3$]PF$_6$, **3**, forms as a deep-red precipitate.[24] Compound **3** is light sensitive and solutions bleach with photoreduction to [(Me$_3$cyclam−acetate)Fe^{II}-(NCCH$_3$)]$^+$ if left in ambient light for even a few hours,[21] so it is important that **3** is crystallized in the dark.

Characterization of the Fe(III) Species. The crystal structures and some of the spectroscopic properties of **2** and **3** have been previously reported, which have shown the molecules to adopt the *trans*-III conformation of the cyclam ligand as shown in Scheme 2.[24]

The spectroscopic properties of **1** in the solid state, for which good crystals could not be obtained, are in agreement with the same structural formulation. The magnetic susceptibility of **1** is shown in Figure 1, where a temperature-independent value of $T = 4.36$ emu K mol^{-1} is seen above 50 K, which is in agreement with the spin only value for an $S = {}^5/_2$ ground state: $\chi T = (1/2)(S(S+1)) = 4.375$ emu K mol^{-1}. Below 50 K, there is a steep decrease in χT, and the value falls below 2 emu K mol^{-1} at 2 K, which exceeds the field saturation behavior expected for the applied field of $B = 1$ *T*, and thus indicates either zero-field splitting or weak intermolecular spin coupling or both. A fit of the data using the spin Hamiltonian given in eq 1 (g is the Landé factor, D is the axial zero-field splitting parameter, β is the Bohr magneton, B is the magnetic field, and S is the spin operator), which only accounts for axial zero-field splitting, results in a value of $D = \pm 10$ cm^{-1}, but this was found to be too large to be in agreement with the EPR and

Table 1. Mössbauer Parameters from Zero-Field Spectra of Frozen Acetonitrile Solutions of the Complexes

compound	δ, mm s^{-1}	ΔE_Q, mm s^{-1}	T, K	ref.
1red	1.08	2.75	80	this work
1red − MeCN bound	1.10	3.49	80	this work
1ox	0.08	2.40	80	this work
2[a]	0.39	0.95	4.2	25
2red	1.11	3.71	80	this work
2ox	0.02	2.43	80	this work
3 − low spin	0.33	2.21	80	24
3 − high spin	0.35	0.84	200	24
3red	1.08	3.17	80	24
3ox	0.11	1.92	80	24

[a] This measurement was done on a solid sample.

Mössbauer data, which both suggest a D value of ~ -4.5 cm^{-1} (vide infra). By fixing the D value to -4.5 cm^{-1} and allowing a Weiss constant to be refined, a successful fit can be obtained, which is the fit shown in Figure 1. The Weiss constant of -1.4 cm^{-1} is most likely due to Fe···Fe antiferromagnetic coupling between iron centers in a chain structure.

$$H = \vec{S}g\beta\vec{B} + \vec{S}\cdot D\cdot\vec{S} \qquad (1)$$

The Mössbauer parameters of all of the species described in this paper are given in Tables 1 and 2 for spectra measured either without or with an applied magnetic field, respectively. The Mössbauer spectrum of a solid sample of **1** at 80 K and no externally applied magnetic field shows considerable spin relaxation with rates that are intermediate to the time scale of the nuclear transition and Larmor precession. The spectrum consists of a broad asymmetric trough from which the isomer shift (δ) and quadrupole splitting (ΔE_Q) are not readily deduced. To determine these parameters, the Mössbauer spectrum of the solid was measured at 4.2 K in a strong applied magnetic field of 7.0 T (see Figure 2a). The spectrum is well resolved but has only weak magnetic splitting typical of a diamagnetic species showing no internal field at the iron nucleus. The values of δ and ΔE_Q could be determined from a simulation with the usual nuclear Hamiltonian and the applied field to be 0.38 and -1.45 mm s^{-1}, respectively, and the asymmetry parameter of the electric field gradient (EFG) tensor, η, is 0.3. The parameters are rather unusual for high-spin Fe(III) coordination compounds; particularly the high quadrupole splitting is remarkable and largely exceeds the values found for the other ferric high-spin species in Table 2. The Mössbauer parameters instead resemble those found for μ-oxo bridged di-iron complexes like the (Me$_3$-cyclam−acetate)FeOFeCl$_3$ starting complex ($\delta = 0.44$ mm s^{-1}, $|\Delta E_Q| = 1.46$ mm s^{-1}), which suggests that the carboxylate should function as a bridging ligand in a chain structure and that at least one of the Fe−O(carboxylate) bonds is quite strong. This may explain also the diamagnetism of the sample found in the spectrum measured at liquid helium temperature. We emphasize that the presence of a true μ-oxo dimer motif can be excluded because such a bridging ligand would mediate strong exchange interaction between the ferric ions of the order 10^2 cm^{-1}, in contrast to the weak interaction found in the magnetic data as well as the paramagnetic relaxation observed in the Mössbauer spectrum recorded at 80 K.

Crystals of **1** are poorly diffracting, and only a rough structure was determined, which is so poor that the data will not be presented here. Nevertheless, the connectivity which appears in the structure is shown in Scheme 3 and it should be noted

Table 2. Parameters from Applied Field Mössbauer Measurements of Complexes in Acetonitrile Solution at 4.2 K

compound	δ, mm s^{-1}	ΔE_Q, mm s^{-1}, η	D, cm^{-1}, E/D	(α, β, γ), deg[d]	g_x, g_y, g_z	(A_{xx}, A_{yy}, A_{zz}), T	ref.
1(solid)[b,c]	0.38	−1.45, 0.3	n.d.	n.d.	n.d.	n.d.	this work
1	0.48	−0.40, 0.7	−4.8(4), 0.10	11, 111, 0	2.00	−22.0, −22.0, −19.5	this work
2	0.39	−0.95, 0.40	+0.4(2), 0.12	−	2.00	−21.3, −21.3, −21.0	25
2red	1.11	+3.71, 0.2	−2.0(2), 0.20	0, −8, 0	2.00	−15.5, −22.5, −13.4	this work
2ox	0.02	+2.45, 0.2	+22.(1), 0	−	2.00	−20.4, −19.1, −2.5[e]	this work
3 − low spin[b]	0.34	−2.28, 0.2	−	0, 66, 0	1.78, 2.26, 2.70	−31.6, +24.8, −49.1	this work
3 − high spin[b]	0.41	−0.93, 0	+4.0(5), 0.3[f]	−	2.00	−20.1[g]	this work
3 − low spin	0.34	−2.43, 0.3	−	0, 69, 0	1.78, 2.26, 2.70	−50.2, +47.4, −5.8	this work
3 − high spin	0.42	−0.32, 0	+2.0(2), 0.3[f]	−	2.00	−20.8[g]	this work
3ox	0.12	+1.92, 0.1	+24.(1), 0.02	−	2.00	−15.4, −17.8, −2.3	24

[a] The experimental errors are typically 0.02 mms^{-1} for δ and ΔE_Q; 0.01 for E/D; 10° for α,β,γ; 0.01 for g values; and 0.1 for A values. Those for D are given in brackets. [b] This measurement was done on a solid sample. [c] In solid samples, **1** does not have an apical Cl$^-$ ligand. [d] These are Euler angles describing rotation of the EFG tensor with respect to the principal axes of the zero-field splitting tensor. [e] The A_{zz} value is not defined. [f] Taken from the EPR measurement of **3** in solution (see Figure 4). [g] Constrained to isotropic values.

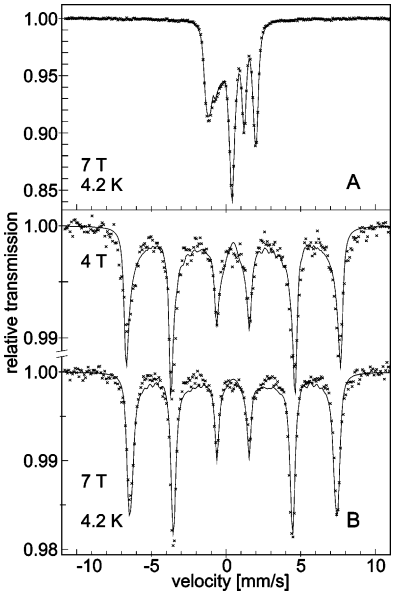

Figure 2. Mössbauer spectra of solid (A) and acetonitrile solutions (B) of **1** taken in applied magnetic field at the field strengths given at 4.2 K. The solid lines represent simulations of the spectra with $S = 0$ for (A) and $S = {}^5/_2$ for (B) and parameters given in Table 2.

Scheme 3

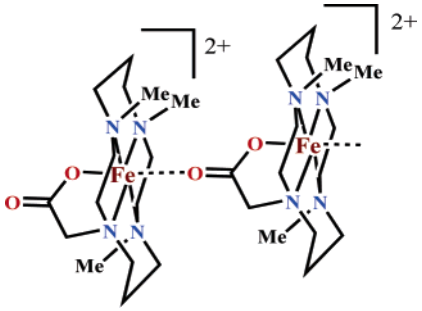

that it appears that the molecules form chains with bridging carboxylate groups, according to the spectroscopic observations. The chloride ions and hexafluorophosphate anions are separated from the positively charged chains.

To break up the antiferromagnetic effects of the chain structure and determine the properties of the individual molecules, the Mössbauer spectrum of **1** was measured in acetonitrile solution (~0.1 mM, 40% enriched with ^{57}Fe). Again, the Mössbauer spectrum at 80 K with no externally applied field was not conducive to interpretation because of intermediate spin relaxation, so two spectra were measured at 4.2 K at externally applied magnetic fields of 4.0 and 7.0 T (Figure 2b,c). These spectra show large paramagnetic hyperfine patterns typical of ferric high-spin ions with large zero-field splitting and were fitted using the spin-Hamiltonian given in eq 2 with $S = {}^5/_2$.

$$H = g\beta\vec{B}\vec{S} + D\left[\vec{S}_z^{\,2} - \frac{1}{3}S(S+1) + E/D(\vec{S}_x^{\,2} - \vec{S}_y^{\,2})\right] + \vec{S}\cdot A\cdot\vec{I} - g_N\beta_N\vec{B}\vec{I} + H_Q \quad (2)$$

Here, g, β, B, S, and D are the same as described in eq 1; E is the rhombicity term of the zero-field splitting tensor, A is the hyperfine coupling tensor, I is the nuclear spin operator, g_N is the nuclear g factor (for ^{57}Fe), β_N is the nuclear magneton, and H_Q is the Hamiltonian describing the quadrupole interaction in the excited-state of the iron (its main parameters being ΔE_Q and η). The wide split hyperfine pattern with narrow lines and distinct intensity ratios reveals the presence of a strong internal field of about 46 T at the Mössbauer nucleus and an "easy axis of magnetization". This is typical of a paramagnetic complex with small rhombicity and a large negative D value, or a fully rhombic system. Because the rhombicity parameter of **1** is found to be small from the EPR spectra, $E/D = 0.1$ (see below), the axial parameter D could be reliably determined from the field dependence of the Mössbauer spectra at 3 and 7 T. The simulations performed in the limit of fast spin relaxation yield $D = -4.8$ cm^{-1}, as well as the components of the hyperfine coupling tensor $A/g_N\beta_N = (-22.0, -22.0, -19.5)$ T, with the anisotropy constraint to axial symmetry. The latter values represent a nearly isotropic hyperfine tensor that is in agreement with the assignment of high-spin Fe(III) in which each d orbital contains one unpaired electron. Finally, the values of δ, ΔE_Q, and η determined from these spectra are 0.48 mm s^{-1}, −0.40 mm s^{-1}, and 0.7, respectively, and are in the range expected for high-spin Fe(III) complexes.

The EPR spectrum of **1** in butyronitrile solution at 10 K is qualitatively similar to that of the corresponding fluoro complex (**2**) and consists of a widely split and broadened $S = {}^5/_2$ signal due to large zero-field splitting exceeding the Zeeman splitting ($D \gg g\beta B$). Resolved derivative signals are observed at effective g values of 8.0, 5.6, and 4.0, which can be assigned to the $|S, m_S> = |{}^5/_2, \pm{}^1/_2>$ Kramers doublet ($g_{eff} = 8$ and 4) and the $|{}^5/_2, \pm{}^3/_2>$ Kramers doublet ($g_{eff} = 5.6$) for a system with a small rhombicity parameter of $E/D \approx 0.1$. The relative intensities at various temperatures in the range 4.2−20 K indicate a negative axial zero-field splitting parameter. The spectrum in Figure S1 was simulated similarly to that of **2**, and the zero-

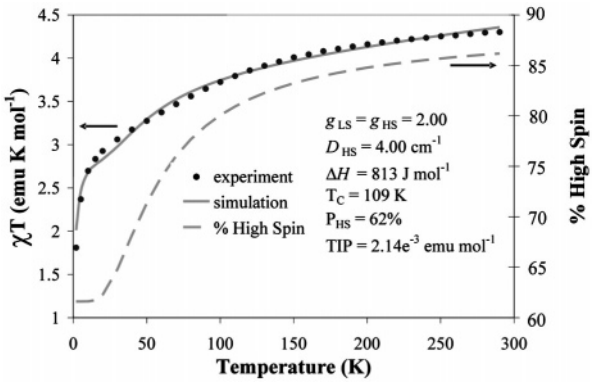

Figure 3. Variable temperature magnetic susceptibility of **3** plotted as χT vs T. The black circles represent the data and the solid line represents a fit of the data as described in the text with the fitting parameters given in the inset. The dashed line is a measure of how much of the sample is high spin based on the simulation and corresponds to the scale on the right-hand side of the plot.

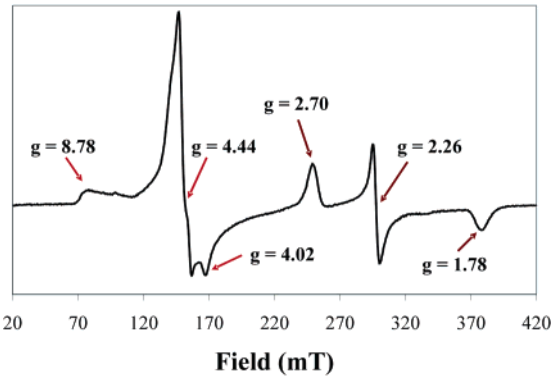

Figure 4. X-band EPR spectrum of **3** in frozen acetonitrile solution in the presence of excess NBu_4PF_6 at 20 K. The major g values are labeled: those for the high-spin species in red, and those for the low-spin species in brown.

field splitting parameters $D = -4.0$ and $E/D = 0.12$ were determined, which are similar to those determined by Mössbauer spectroscopy (vide supra).

The properties of **2** have been previously reported[25] as have some of the properties of **3**,[24] although we present here a more detailed discussion of **3**, with particular emphasis on its spin-crossover behavior. The unusual temperature dependence of χT found for **3** (Figure 3) is reproducibly observed in several experiments and is a result of spin crossover. At room temperature, the χT value is 4.3 emu K mol^{-1}, very close to the spin-only value expected for an $S = {}^5/_2$ system (4.375 emu K mol^{-1}). This value drops fairly steadily as the temperature is decreased, ultimately reaching a value of ~ 2 emu K mol^{-1} at the lowest temperatures measured (2 K). This behavior can be modeled as arising from a variety of different sources such as zero-field splitting or intermolecular spin pairing, and indeed a hypothetical fit of the magnetic susceptibility data with the spin Hamiltonian given in eq 1 treating only axial zero-field splitting gives a reasonable fit of the data, but a zero-field splitting value D which is unphysically large ($D = \sim 50$ cm^{-1}).

The fact that a spin-crossover phenomenon is involved is best seen in the EPR and Mössbauer spectra of the compound (vide infra), in which both high-spin and low-spin components are seen at low temperatures. On the basis of this information, it is reasonable to simulate the susceptibility data in Figure 3 with an ideal solution spin crossover model which also includes the zero-field splitting of the high-spin state, as in eq 3.

$$\chi T = (1 - P_{HS})\left(\frac{F_{HS} - F_{LS}}{1 + \exp\left(\frac{\Delta H}{R}\left(\frac{1}{T} - \frac{1}{T_C}\right)\right)} + F_{LS}\right) + P_{HS}F_{HS} \quad (3)$$

Here, F_{HS} is a function simulating the high-spin species based on eq 1 with $g = 2.00$, and $D = 4.00$ cm^{-1} (also including a temperature-independent paramagnetism component of 2.14×10^{-3} emu K mol^{-1}), F_{LS} is a function simulating the low-spin species with $g = 2.00$, ΔH is the enthalpy difference between the high- and low-spin states, R is the gas constant, T_C is the critical temperature (i.e., the temperature at which equal amounts of high- and low-spin species are present in the portion of the sample that undergoes spin crossover), and P_{HS} is the amount of the sample that remains high spin over the whole temperature range. The functions F_{HS} and F_{LS} were not refined, and their corresponding g and D values were fixed to the values given above. The optimized parameters were ΔH, T_C, and P_{HS}, which refined to the values given in the inset to Figure 3. The enthalpy difference is $\Delta H = 813$ J mol^{-1} and may be used to calculate the ΔS of the spin crossover process ($\Delta H = T_C\Delta S$), which is 7.5 J mol^{-1} K^{-1}. It should be noted that 62% of the sample does not undergo spin crossover and remains high spin in the entire temperature range, and this agrees well with the Mössbauer spectrum of the solid at 4.2 K (vide infra). Although it is unusual that a portion of the sample remains high spin, it is not without precedent, and several examples of similar systems are known in the literature.[32−37]

Compound **3** shows a sharp EPR spectrum in frozen acetonitrile solution in the presence of NBu_4PF_6. The spectrum, shown in Figure 4, can be thought of as having two main components, one having signals at $g_{eff} = 9.0$, 4.4, and 4.0, and the other having signals at $g = 2.70$, 2.26, and 1.78. The g values of the latter species are in good agreement with a low-spin iron(III) formulation (and have a larger anisotropic spread than the g values of [(cyclam−acetate)FeN_3]PF_6, which are 2.55, 2.26, and 1.91), whereas the higher g_{eff} values of the former species clearly indicate a species with a higher total spin, and these may be assigned to the high-spin species.[38]

It is remarkable that both high- and low-spin species are observed in the solution spectra because it means that: a. **3** undergoes spin crossover in frozen solution (not just in the solid state), b. as was seen in the solid-state susceptibility measurements, the spin crossover is incomplete and a good portion of the sample remains high spin at low temperatures, and c. relaxation between the two spin states is slow relative to the

(32) Terzis, A.; Filippakis, S.; Mentzafos, D.; Petroulleas, V.; Malliaris, A. *Inorg. Chem.* **1984**, *23*, 334.
(33) Timken, M. D.; Hendrickson, D. N.; Sinn, E. *Inorg. Chem.* **1985**, *24*, 3947.
(34) Chun, H. P.; Bill, E.; Weyhermüller, T.; Wieghardt, K. *Inorg. Chem.* **2003**, *42*, 5612.
(35) Chun, H.; Weyhermüller, T.; Bill, E.; Wieghardt, K. *Angew. Chem., Int. Ed.* **2001**, *40*, 2489.
(36) Ryabova, N. A.; Ponomarev, V. I.; Zelentsov, V. V.; Atovmyan, L. O. *Kristallografiya* **1982**, *27*, 279.
(37) Ryabova, N. A.; Ponomarev, V. I.; Zelentsov, V. V.; Atovmyan, L. O. *Kristallografiya* **1982**, *27*, 81.
(38) Simulation of the high-spin species has thus far not been possible because the signals at 9.0, 4.4, and 4.0 do not correspond to any of the expected transitions based on the rhombogram for an $S = {}^5/_2$ system, though they are somewhat near the transitions expected for the fully rhombic case ($E/D = 0.33$ having $g_{eff} = 9.6$ and 4.3). It is also possible that these signals arise from a weakly coupled dimer of spin ${}^5/_2$ centers, though preliminary simulations are not conclusive. A Q-band spectrum of this species was also measured, but the general shape of the spectrum is the same.

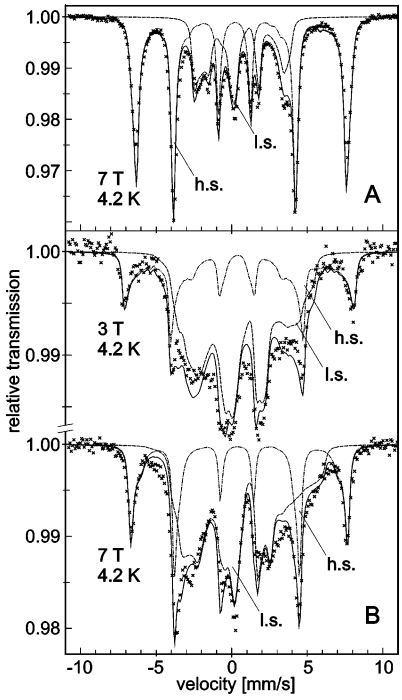

Figure 5. Mössbauer spectra of solid **3** (A) and in acetonitrile solutions (B) taken in applied magnetic field at the field strengths given at 4.2 K. The lines represent simulations of the spectra with spin $S = {}^5/_2$ for the high-spin component (dashed-dotted line, labeled h.s.), $S = {}^1/_2$ for the low-spin component (dashed line, labeled l.s.), and parameters as given in Table 2. The high-spin contribution is calculated in the slow-relaxation limit in the solid (A), 67% relative intensity, and in fast relaxation in solution (B), 30% relative intensity. From the low-spin component, spin relaxation was found to be fast in the solid (A) but slow for the solution (B).

time scale of EPR (and also relative to the Mössbauer time scale (*vide infra*)).

Both high- and low-spin species are seen in the low-temperature Mössbauer spectra of **3** taken either on the solid or on a frozen solution. At 200 K, an acetonitrile solution of **3** shows a single asymmetric quadrupole doublet (with approximately $\delta = 0.35$ mm s^{-1}, $\Delta E_Q = 0.84$ mm s^{-1}) characteristic of a high-spin ferric species, but at 80 K, two doublets are observed which were deconvoluted, one having the same Mössbauer parameters as above and the other having a slightly lower δ of 0.33 mm s^{-1} and a larger ΔE_Q of 2.21 mm s^{-1}, both indicative of low-spin Fe(III).[24] An applied-field (7 T) Mössbauer spectrum of solid **3** at 4.2 K was obtained which shows a complex pattern (Figure 5, top). Knowing the ratio of high- and low-spin components from the susceptibility measurement, it is possible to deconvolute this Mössbauer spectrum into two parts, one for the high-spin species (accounting for roughly 60% of the total iron in the sample) and one for the low-spin species (accounting for the remaining 40%).

The six most intense lines in the spectrum can be easily ascribed to the high-spin component by their large magnetic splitting indicating an internal field of about 45 T, and by comparison with the applied field Mössbauer spectra of **1** and **2**. Spin Hamiltonian analysis of this subspectrum yields the parameters given in Table 2, and it should be noted here that δ and ΔE_Q of 0.41 and -0.93 mm s^{-1}, respectively, agree well with the formulation as high-spin Fe(III) and are similar to the values found in the Mössbauer spectra of **1** and **2**. The same is true for the hyperfine tensor components. It should also be noted that the ΔE_Q values for all three high-spin species **1**, **2**, and **3** are negative, implying that the shape of the EFG tensor is elongated along the O−Fe−X axis of the molecule. This is in contrast to what is seen for ferric high-spin porphyrin species, where the sign of ΔE_Q is nearly always positive, an effect which we believe to be due to the π bonding capability of porphyrin ligands which Me$_3$cyclam−acetate lacks.

With the high-spin subspectrum well defined, it is possible to simulate the minor subspectrum with an $S = {}^1/_2$ model using the g values taken from the EPR spectrum and the δ and ΔE_Q values from the zero-field spectrum, which allows the asymmetry parameter of the EFG tensor, η, and the hyperfine splitting tensor components to be refined. Like its low-spin non-methylated cyclam−acetate analog, [(cyclam−acetate)FeN$_3$]PF$_6$, the ΔE_Q value of **3** is negative ($\Delta E_Q = -2.28$ mm s^{-1}, $\eta = 0.2$ for **3**; $\Delta E_Q = -2.53$ mm s^{-1}, $\eta = 0.40$ for [(cyclam−acetate)-FeN$_3$]PF$_6$[18]), and the hyperfine tensor components are highly anisotropic ranging from −49.1 to +24.8 T in **3**. In [(cyclam−acetate)FeN$_3$]PF$_6$, the range is from −41.2 to +35.0 T,[18] and in both complexes the A_{yy} component is positive and the other two components are negative.

An applied field Mössbauer spectrum of **3** was also taken on a frozen solution of **3** in acetonitrile at 4.2 K (Figure 5, bottom), which is similar in complexity to the spectrum of the solid. Again, both high- and low-spin components are observed, although the ratio of the two species here is roughly 30:70. For the high-spin subspectrum, the refined parameters (Table 2) are all quite similar to those observed in the solid except that the value of ΔE_Q appears to be decreased. In the low-spin subspectrum, however, the values of the A tensor vary more (from −50.17 to + 47.44 T), though the general pattern that $A_{yy} > 0$; A_{xx}, $A_{zz} < 0$ is still true.

The spectroscopic data for the low-spin species warrants further discussion. The anisotropy of the g values may be interpreted in terms of the ligand field model developed by Griffith[39] and Taylor[40] for description of the 3d^5 low-spin configuration in octahedral symmetry. Analysis of the g values yields a ground state with ~ 97% $(d_{xy})^2(d_{xz}, d_{yz})^3$ character and in this analysis we have chosen the y-axis to be the unique axis (implying a hole in the d_{yz} orbital). The splitting Δ/λ between the (d_{xz}, d_{yz}) and d_{xy} orbitals is 4.58, with a rhombic splitting between the d_{xz} and d_{yz} orbitals of $V/\lambda = 2.82$, where λ is the spin orbit coupling parameter. The resulting valence contribution to the EFG arising from the d_{yz} orbital has its main component along the y direction. This agrees with the spin Hamiltonian analysis of the magnetic Mössbauer spectrum in which the Euler angle $\beta \approx 70°$ is found, which is close to the expected value of $\beta = 90°$ to rotate V_{zz} (the main component of the EFG tensor) into the y-axis. The spin-dipolar contribution to the anisotropy of the magnetic hyperfine tensor A may also be predicted within this ionic picture. The estimate yields a positive component for A_{yy} and negative values for A_{xx} and A_{zz} which fits the experimental result. Moreover, this general picture agrees with the previous analysis of [(cyclam−acetate)FeCl]PF$_6$ and [(cyclam−acetate)FeN$_3$]PF$_6$, though the t_{2g} splitting in low-spin **3** is less rhombic than for the non-methylated azido species ($\Delta/\lambda = 5.7$, $V/\lambda = 3.9$) and resembles more the nonmethylated chloro complex ($\Delta/\lambda = 4.84$, $V/\lambda = 2.39$). The difference in the two azido species likely arises from a difference in the Fe−N−N

(39) Griffith, J. S. *Proc. R. Soc. London, Ser. A.* **1956**, *235*, 23.
(40) Taylor, C. P. S. *Bichimica Biophysica Acta.* **1977**, *491*, 137.

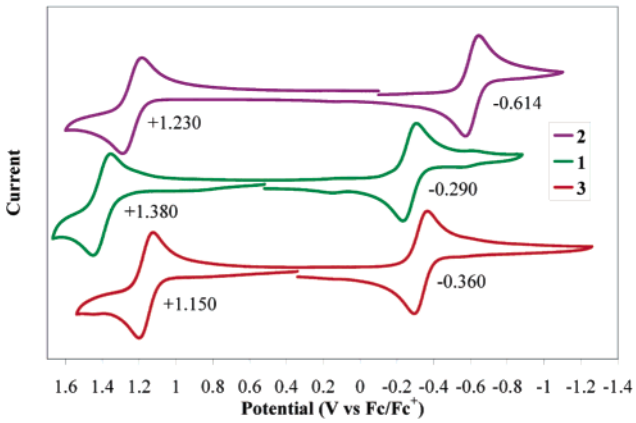

Figure 6. Cyclic voltammograms of **1**, **2**, and **3** in acetonitrile with 0.1 M NBu_4PF_6 supporting electrolyte. The numbers next to each wave are their corresponding $E_{1/2}$ values in *V* vs ferrocene/ferrocenium.

Table 3. Electrochemical Data[a] for Cyclam−Acetate and Me_3cyclam−Acetate Complexes

compound	$Fe^{2+/3+}$ $E_{1/2}$, V	$Fe^{3+/4+}$ $E_{1/2}$, V	ref.
[(cyclam−acetate)FeCl]PF_6	−0.640	1.330 (irreversible)	18
[(cyclam−acetate)FeN_3]PF_6	−0.750	0.990 (irreversible)	18
1	−0.290	1.380	this work
2	−0.614	1.230	this work
3	−0.360	1.150	24

[a] Solvent: MeCN; all potentials are referenced vs the ferrocene/ferrocenium couple.

angle in the two species; in **3**, the additional methyl groups may not allow this angle to become as acute as is found in [(cyclam−acetate)FeN_3]PF_6 (132 °).

Electrochemically, **1**, **2**, and **3** behave similarly in acetonitrile solutions. Their respective cyclic voltammograms are shown in Figure 6, and their redox potentials are collected in Table 3 along with those of the analogous cyclam−acetate complexes. Notably, whereas the complexes of cyclam−acetate show only irreversible waves corresponding to the $Fe^{3+/4+}$ process, this process is reversible for *all three* complexes of Me_3cyclam−acetate. Compounds **1** and **3** are more easily reduced than their non-methylated analogs by 350−400 mV, which is in agreement with the difference in spin state between the two species and agrees with the observations of the Meyerstein group on the weaker donor strength of *N*-alkylated cyclam ligands.[26] In contrast to the greater stability of the ferrous species in the complexes of Me_3cyclam−acetate, which is a thermodynamic effect, the reversibility of the $Fe^{3+/4+}$ couple in these complexes represents a kinetic stability of the Fe^{4+} species.

Of the three methylated complexes, the fluoro complex **2** is the most difficult to reduce, which agrees well with the fact that the fluoride ion, a very hard base, prefers to form a strong bond to the ferric ion, which is a harder acid than the ferrous ion. The oxidation potentials increase in the series **3** > **2** > **1**, which may be considered a measure of how well each of the three axial ligands stabilizes the tetravalent iron center. The fact that the oxidation potential of the chloro complex is the highest may also in part be due to steric crowding. The chloro anion may not be able to form a short bond to the iron because it could be hindered by the methyl groups. Indeed, we believe this to be the main reason for the relative kinetic instability of the Fe(IV) chloro complex (vide infra). Coulometric reduction and oxidation of **1**, **2**, and **3** allow study of the Fe(II) and Fe(IV) species by various techniques, the results of which are detailed below.

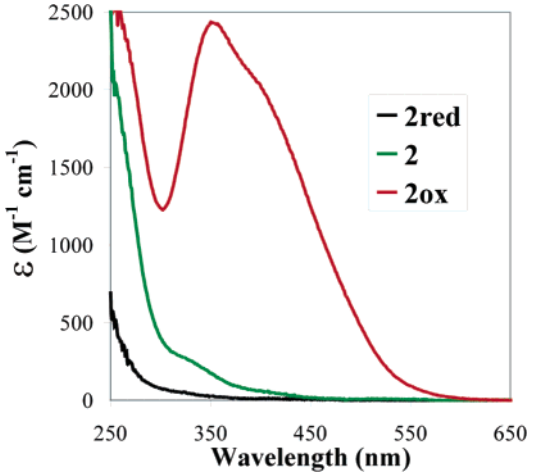

Figure 7. Electronic spectra of **2red**, **2**, and **2ox** obtined during controlled potential coulometry.

Characterization of the Fe(II) Species. The reduction products of **1**, **2**, and **3** were investigated by spectroelectrochemistry in the UV−vis region. The electronic spectra for **3red**, **3**, and **3ox** have been previously reported,[24] and those for **2red**, **2**, and **2ox** are shown in Figure 7. As seen from these spectra, solutions of **2red** and **3red** are colorless, and **1red** is no different. The lack of color indicates that the bands originating from the $^5T_{2g}\rightarrow{}^5E_g$ transition of the ferrous ion must occur at >1000 nm. Also, any charge-transfer bands from the acetate or axial groups to the iron are shifted significantly into the UV.

Compounds **2** and **3** were also studied by infrared spectroelectrochemistry because in both compounds, very intense and important stretches are found in regions of the spectrum which are not obscured by the solvent (acetonitrile) or electrolyte (tetrabutylammonium hexafluorophosphate). Compounds **2** and **3** have carbonyl stretches at 1680 and 1677 cm^{-1}, respectively. In compound **3**, an intense band at 2090 cm^{-1} is also present which is the azido stretch. Infrared spectra of **3red**, **3**, and **3ox** are shown in Figure 8, which display both of these stretches as well as some of the absorptions of the solvent and electrolyte, which emphasize the limitations of these measurements. The values highlighted in Figure 8 for the N_3 and C═O stretching are also given in Table 4 along with the corresponding values from **2** and its derivatives. In both cases, the C═O stretch shifts to lower frequency upon reduction to Fe(II), which is in agreement with there being a weaker Fe−O bonding interaction in the ferrous state and therefore more π-delocalization within the carboxylate moiety. The azido stretch in **3red** is also observed at lower frequency than the corresponding band in **3**, indicating stronger π interactions between the azide ligand and the ferrous ion than is observed in the case of the ferric ion.

The reduction products of **1**, **2**, and **3** have also been studied by Mössbauer spectroscopy by using electrochemically reduced samples of **1**, **2**, and **3** enriched 40% in ^{57}Fe. Reduction of **1** is complex. The Mössbauer spectrum of coulometrically reduced **1** shows two overlapped doublets (Figure S2) having the following parameters (see Table 1): $\delta_1 = 1.08$ mm s^{-1}, $\Delta E_{Q1} = 2.75$ mm s^{-1}; $\delta_2 = 1.10$ mm s^{-1}, $\Delta E_{Q2} = 3.49$ mm s^{-1}.

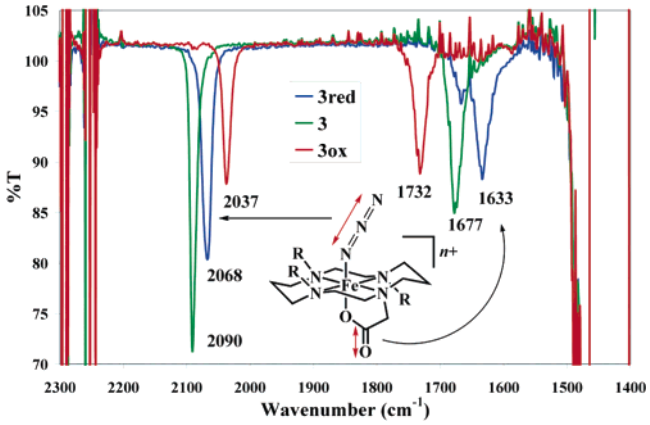

Figure 8. Infrared spectra of **3red**, **3**, and **3ox** (with the charge $n = 0$, 1, or 2, respectively) in the region between 1400 and 2300 cm^{-1} taken during chronoamperometry to generate the Fe(II) and Fe(IV) species. The dominant bands at 2300, 2250, and 1500−1400 cm^{-1} are absorptions of the solvent and electrolyte, shown to emphasize the limited window of the system. Numbers next to each band are the frequencies of the peaks, and a diagram of the molecule is shown in the inset, highlighting the two different absorptions seen.

Table 4. IR Data for **2red**, **2**, **2ox**, **3red**, **3**, and **3ox**

	C=O stretch, cm^{-1}	N_3 stretch, cm^{-1}	reference
2red	1630		this work
2	1680		this work
2ox	1753		this work
3red	1633	2068	24
3	1677	2090	24
3ox	1732	2037	24

Both species may be assigned to high-spin Fe(II) complexes due to their large isomer shifts and quadrupole splittings. Because the two species have similar Mössbauer parameters, they are also presumed to be structurally very similar, and it is proposed that both are six-coordinate and that one species contains an axial chloro ligand whereas in the other, this ligand has been replaced by acetonitrile.[41] This proposal, however, presents the problem of determining which species is actually **1red** and which is the acetonitrile-bound species. To determine this, reduction of **1** was undertaken in acetonitrile with a mixture of electrolytes. A 0.1 M electrolyte solution was used, but instead of using NBu_4PF_6 as before, a mixture of 9:1 NBu_4PF_6 and NBu_4Cl was used, which provides a large excess of chloride ions in solution. The Mössbauer spectrum of the resulting reduced species shows only one major signal having the same parameters as species 1 above, clearly identifying this species as **1red**.

The reactions involved in the above discussion are represented in Scheme 4, which also shows that a pre-equilibrium between **1** and an acetonitrile-bound Fe(III) species may also occur, but to only a small extent. The loss of chloride in **1red** is believed to be due mainly to steric reasons, but also due to the fact the Cl−Fe(II) bond will be weaker than the Cl−Fe(III) bond for electrostatic reasons.

In contrast to this behavior, reduction of **2** and **3** give cleanly one product as seen in their Mössbauer spectra. The spectrum of **3red** was previously reported and is consistent with the formulation of high-spin Fe(II), and the spectrum of **2red** is

(41) An alternative proposal is that one species is five-coordinate, but this should lead to a much larger quadrupole splitting whereas the quadrupole splittings observed are similar to those of the six-coordinate species **2red** and **3red**.

Scheme 4

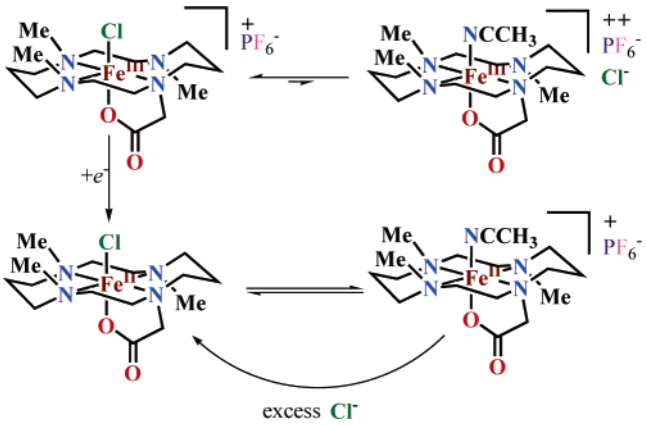

shown in Figure S3 along with a spectrum of the same sample measured in an applied magnetic field of 7 T. This was simulated using the spin Hamiltonian analysis (see eq 2) for $S = 2$, resulting in the parametrized values given in Table 2. The electronic g values were fixed to be equal to 2.[42]

Characterization of the Fe(IV) Species. Coulometric oxidation of **1** at a potential of ∼1.5 V vs ferrocene/ferrocenium was monitored by the changes in the UV−vis spectrum. For a simple electron-transfer process (e.g., **1** → **1ox** + e^-) the changes in the UV−vis spectrum should be isosbestic during the entire coulometry as the spectrum of **1** disappears and the spectrum of **1ox** appears. In practice, however, isosbestic behavior is seen during the first ∼100−200 s of the coulometry, but the newly appearing band at 460 nm thereafter loses intensity nonisosbestically. From this experiment it is apparent that the oxidation product **1ox** is not stable and decomposes during the time of the coulometry (even though the coulometry was carried out at −25 °C). Thus, it was not possible to produce a pure sample of **1ox** for spectroscopic study, but an aliquot of the reaction mixture taken during the coulometry but before decomposition was frozen and a Mössbauer spectrum was measured at 80 K (see Figure S4) where two species are clearly observable. The main signal is broad and ill defined and is typical of the high-spin ferric species **1**, but a sharp quadrupole doublet is also observed with the parameters $\delta = 0.08$ mm s^{-1} and $\Delta E_Q = 2.40$ mm s^{-1}. These are assigned as the Fe(IV) species **1ox**. Notably, the quadrupole splitting is somewhat larger than that observed for **3ox** (for which $\Delta E_Q = 1.92$ mm s^{-1}).[24]

We propose two possible reasons for the instability of **1ox**. The first is that the chloride ion may be an ineffective axial ligand for the complex because of its size. As discussed above, the chloride ion can be fairly easily removed in the ferrous and ferric complexes and may not be able to bind closely to the Fe(IV) center because of the steric effects of the methyl groups. Another consideration is that the electrode potential is very high for the coulometric process, and if the equilibrium shown at the top of Scheme 4 produces any free chloride ions in solution, these may be oxidized to chlorine either by the electrode or perhaps by **1ox** itself. These points are interesting considering the stability of a chloro-Fe(IV) complex, synthesized by Collins et al.[43] and of (corrole)FeCl species may may contain the Fe(IV) ion.[7]

(42) The A and D values determined in this fit are not unambiguously defined and should be considered to be approximately correct.
(43) Collins, T. J.; Kostka, K. L.; Münck, E.; Uffelman, E. S. *J. Am. Chem. Soc.* **1990**, *112*, 5637.

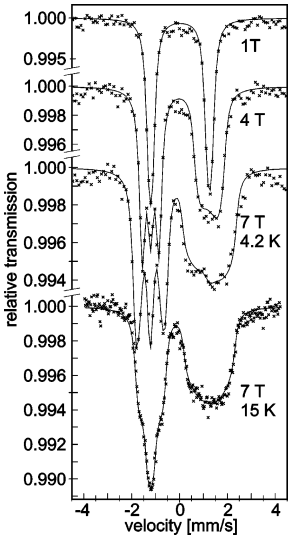

Figure 9. Mössbauer spectra of **2ox** in acetonitrile solution taken in applied magnetic field at the field strengths given at 4.2 K (top three) and 15 K (bottom trace). The solid lines represent spin Hamiltonian simulations for $S = 1$, assuming fast spin relaxation with the parameters given in Table 2.

Coulometric oxidation of **2** yields a pale-orange solution,[44] the electronic spectrum of which is shown in Figure 7. Here, the intense bands in the visible region at 420 and 360 nm are likely charge-transfer bands (acetate to iron charge transfer) which are low enough in energy to be observed in the visible region. They are assigned as such due to the fact that they occur in **1ox**, **2ox**, and **3ox** and therefore are not altered when the axial ligand is exchanged. The decrease in energy of these charge-transfer bands correlates nicely with the expected shortening of the Fe−O distance (vide infra) in the complex as the oxidation state increases. The observed shifts in the C═O stretching band in the IR spectrum (Table 4) also agree well with this interpretation, as will be discussed further below.

The Mössbauer spectrum of a frozen acetonitrile solution of **2ox** prepared coulometrically consists of a single doublet with $\delta = 0.02$ mm s^{-1} and $\Delta E_Q = 2.43$ mm s^{-1}, which agree with the assignment of the oxidation as being iron centered. Comparing these data to those of **1ox** and **3ox**, the isomer shift values of the complexes decrease in the series as the axial ligand is changed: F < Cl < N_3. Because the isomer shift is directly related to the electron density at the iron nucleus, this may be taken as an indication of the π donating ability of the axial ligands F, Cl, and N_3. Spectra of **2ox** were also measured in applied magnetic fields of 1, 4, and 7 T at 4.2 K and also an additional spectrum at 15 K and 7 T was measured (see Figure 9). The 4.2 K spectra show only limited magnetic splitting, indicating an integer spin ground state with fairly large positive zero-field splitting (resulting in an $m_S = 0$ state lowest in energy). Because **2ox** could be either high spin ($S = 2$) or low spin ($S = 1$), and both of these possibilities may result in an $m_S = 0$ ground state, both possibilities were employed to fit the data. It was found that only the $S = 1$ model could account for the splitting of the left line of the quadrupole doublet into three lines, so the $S = 2$ model was discounted. The fourth spectrum at 15 K was then measured so that a more precise determination of the zero-field splitting tensor could be made. The fit shown in the solid lines in Figure 9 is the result, but it is unfortunately not a unique fit because the value of A_{zz} is undefined (any value for A_{zz} results in an identical simulation of the spectrum) and D is correlated with E/D.[45] Thus, only the relative magnitude of D can be determined for **2ox**, but this is in good agreement with the value determined for **3ox**.

The spectroscopic details of **3ox** have been described previously; it is an octahedral Fe(IV) species with an $S = 1$ ground state which has several absorptions in the UV−vis region at ∼330, 430, 540, and 650 nm. Interestingly, when **3ox** is irrradiated with laser light at 650 nm in frozen acetonitrile solution, the yellow diamagnetic dication $[(Me_3cyclam-acetate)FeN]^{2+}$ is formed, which is a genuine Fe(VI) species (d^2, $S = 0$) via photooxidation producing also one equivalent of dinitrogen.[21]

Calculations on the Electron-Transfer Series $[(Me_3cyclam-acetate)FeF]^{0/+/2+}$. We previously reported calculations[25] using density functional theory (DFT) on the cation from **2**, namely, $[(Me_3cyclam-acetate)FeF]^+$. These results shall be compared here with new results for $[(Me_3cyclam-acetate)FeF]^0$ and $[(Me_3cyclam-acetate)FeF]^{2+}$ to gain more insight into the geometric and electronic structures of these species. The optimized geometry for $[(Me_3cyclam-acetate)FeF]^+$ was taken as a starting point for geometry optimizations of the ferrous and Fe(IV) species, and the main geometric results are collected together in Table 5.[46] The calculated geometry of the ferric species is in good agreement with the known structure of **2**, with the exception that the Fe−N distances are overestimated by the calculation;[25] therefore, reasonable agreement between the calculated and actual geometries of the Fe(II) and Fe(IV) species is expected, even though the exact structures of these are not yet known. As expected, all of the iron-ligand bond distances decrease upon increasing the oxidation state of the iron due to the increased charge on the metal. All of the calculated structures can be described as consisting of an octahedrally coordinated iron center with an axially compressed ligand surrounding. The Fe−F bond is in each case the shortest metal−ligand bond in the molecule and becomes shorter by 0.07 to 0.10 Å per increase in the oxidation state of the iron resulting in a steady increase in the calculated Fe−F bond order (Table 6). The corresponding change in the Fe−O distance is 0.13 to 0.15 Å, and the change in the average Fe−N distances is not as drastic between the ferrous and ferric complexes but is calculated to be ∼0.10 Å from ferric to Fe(IV). Interestingly, the average Fe−N distance never falls below 2.1 Å, even in the low-spin Fe(IV) structure, which is likely a result of the steric effects of the methyl groups in the complex that cause the Fe−N bonds to be longer than one would expect. This is nicely shown by geometry optimization of the corrosponding Fe(IV) fluoro complex of the cyclam−acetate ligand (a hypothetical molecule), which has N−H groups instead of N−Me groups. This model converges to a structure having Fe−N bond distances of 2.053 Å, 0.06 Å shorter than in the methylated complex.

(44) In this case, it was found to be necessary to perform the oxidation at −40 °C and in a glassy carbon vessel to prevent decomposition.

(45) In addition to the parameters from the axial model listed in Table 2, an alternate simulation with $D = 24.7$ cm^{-1}, $E/D = 0.33$ (the rhombic limit) is also possible. In this case, the A values change to {−28.4, −16.0, −3.6} T.

(46) The calculations were performed using two different basis sets of double-ζ and triple-ζ quality. Though changing the basis set results only in minor differences in the resulting geometries, for practical purposes, the results of only the triple-ζ calculations shall be used in our discussion.

Table 5. Geometric Data[a] for Calculated Structures of the $[(Me_3cyclam-Acetate)FeF]^{n+}$ Series, $n = 0, 1, 2$

	2 (exp.)[b]	$(Me_3cyclam-acetate)FeF$ $S=2$	$[(Me_3cyclam-acetate)FeF]^{+}$ $S=5/2$[b]	$[(Me_3cyclam-acetate)FeF]^{2+}$ $S=1$	$[(Me_3cyclam-acetate)FeF]^{2+}$ $S=2$
Fe−F, Å	1.848(2)	1.933	1.871	1.766	1.766
Fe−N_{av}, Å	2.148[2]	2.248	2.221	2.115	2.201
Fe−O, Å	1.979(2)	2.087	1.959	1.800	1.803
O−Fe−F, deg	175.5(1)	172.1	168.6	174.8	172.9
Δd(Fe−N_4), Å[c]	0.099	0.132	0.079	0.036	0.071
E, rel., kJ mol^{-1}				0	+50

[a] Reported values are from calculations with BP86/TZVP. Geometries using SV(P) given in Table S1. [b] Data taken from ref 25. [c] This is the distance of the iron atom above the plane formed by the four amine nitrogen atoms.

Table 6. Calculated and Experimental Spectroscopic Properties of **2**, **2red**, and **2ox**

	2red	$(Me_3cyclam-acetate)FeF$	**2**	$[(Me_3cyclam-acetate)FeF]^{+}$	**2ox**	$[(Me_3cyclam-acetate)FeF]^{2+}$	
$2S+1$	5	5	6	6	3	3	5
Fe 3d spin density	−	3.66	−	4.18	−	2.14	3.57
Fe−F bond order[a]	−	0.5684	−	0.6783	−	0.8599	0.8569
ν(C═O), cm^{-1}	1630	1663	1682	1706	1753	1770	1765
$g$iso	2.00[b]	2.034	2.00	2.010	2.00[b]	2.044	2.015
D, cm^{-1}, E/D	−2.00, 0.20	−1.74, 0.045	+0.4, 0.12	+0.898, 0.037	+21.9, 0	+5.62, 0.029	+10.3, 0.324
δ, mm s^{-1}	1.11	0.99	0.39	0.43	0.02	0.086	0.102
ΔE_Q, mm s^{-1}, η	+3.71, 0.15	+2.83, 0.136	−0.95, 0.4	−1.22, 0.29	+2.43, 0	+2.31, 0.04	+0.474, 0.528
A, MHz	{−21.4, −31.0, −18.5}	{−21.54, −38.41, −39.36}	{−29.4, −29.4, −29.0}	{−31.3, −31.9, −32.0}	{−15.2, −13.8, 0[c]}	{−4.1, −33.0, −33.3}	{−24.6, −25.7, −31.7}

[a] Calculated from Löwdin analysis. [b] Fixed in simulation of the Mössbauer spectra. [c] Value could not be determined.

In the crystal structure of **2**, the position of the iron atom is somewhat out of the equatorial plane formed by the four nitrogen atoms of the cyclam ring, pulled 0.099 Å out of this plane away from the acetate ligand (as calculated from a dummy position at the center of the mean plane described by the four N atoms). This distortion is likely due to the mismatch between the cavity size of the Me_3cyclam−acetate ligand and the ionic radius of the ferric ion. The calculated structures of $(Me_3cyclam-acetate)FeF$, $[(Me_3cyclam-acetate)FeF]^{+}$ and $[(Me_3cyclam-acetate)FeF]^{2+}$ reproduce this distortion, which shall be called Δd(Fe−N_4), and the value of Δd(Fe−N_4) for the calculated ferric structure (0.079 Å) is in good quantitative agreement with the crystal structure of **2** (Δd(Fe−N_4) = 0.099 Å). The calculated values of Δd(Fe−N_4) increase as the oxidation state of the iron is lowered, and hence as the ionic radius of the iron ion increases. In the ferrous species, the Fe−N bond distances increase by only 0.02 Å as compared to the ferric species, which may indicate the limit of how much the cyclam ring can stretch to accommodate the large radius of the high-spin ferrous ion, which is consequently pushed significantly out of the N_4 plane by 0.13 Å. The Fe(IV) ion is much smaller, and fits well into the cavity of the Me_3cyclam−acetate ligand with only a small Δd(Fe−N_4) of 0.036 Å. It should be mentioned that the crystal structure of **3** shows no distortion, but this may be an artifact due to the fact that the iron atom in **3** lies on a crystallographic center of inversion and is therefore required to have a Δd(Fe−N_4) of 0 Å.

An advantage of DFT is the ability to calculate the properties of hypothetical molecules or real molecules with a different electronic structure from that observed in their ground state. Using this approach, the Fe(IV) species $[(Me_3cyclam-acetate)FeF]^{2+}$ was calculated in the unobserved high-spin state ($S = 2$), so that more information about the electronic structure and spin energetics of octahedral Fe(IV) complexes could be gained. Geometrically, the structure of high-spin $[(Me_3cyclam-acetate)FeF]^{2+}$ is similar to the analogous low-spin structure, with the exception that the average Fe−N distance of 2.201 Å is nearly 0.1 Å longer for the former, as has been previously noted in calculations of low-and high-spin Fe(IV)═O species.[47,48] This is easily understood considering a simple ligand field model for the d^4 Fe(IV) ion, which in an axially compressed octahedral geometry will have the configuration $(d_{xy})^2(d_{xz})^1(d_{yz})^1$ for the low-spin state and $(d_{xy})^1(d_{xz})^1(d_{yz})^1(d_{x^2-y^2})^1$ for the high-spin state, where now there is an electron in the $d_{x^2-y^2}$ orbital that is strongly antibonding with respect to the equatorial nitrogen atoms. Energetically, the high-spin state is calculated 50 kJ/mol above the ground triplet state (calculated from B3LYP).

The above trend in the orbital population as well as the trends for the ferric and ferrous species are summarized in Figure 10, which shows a semi-qualitative energy diagram (energies are based on the calculated energies of quasi-restricted orbitals for each case[48]) of the d orbitals and their occupancies across the series from high-spin Fe(II) to low-spin Fe(III), high-spin Fe(III), low-spin Fe(IV), and high-spin Fe(IV). UHF natural orbitals for the low-spin Fe(IV) species are shown in the right side of the Figure.

For all species, the iron d orbitals have energies which increase in the order $d_{xy} < d_{xz} \approx d_{yz} < d_{x^2-y^2} < d_{z^2}$, as expected from ligand field theory. Another qualitative prediction from ligand field theory is that as the oxidation state of the metal is increased, so too is the value of $10Dq$. This is also in good agreement with the results seen in Figure 10, as the energy separation between the d_{xy} and d_{z^2} orbitals increases by 14% between high-spin Fe(II) and high-spin Fe(III), and by 38% between high-spin Fe(III) and low-spin Fe(IV). This result correlates well with the more dramatic change in the iron-ligand bond distances between the $Fe^{III/IV}$ couple as compared to the $Fe^{II/III}$ couple.

(47) Neese, F. *J. Inorg. Biochem.* **2006**, *100*, 716.
(48) Schöneboom, J. C.; Neese, F.; Thiel, W. *J. Am. Chem. Soc.* **2005**, *127*, 5840.

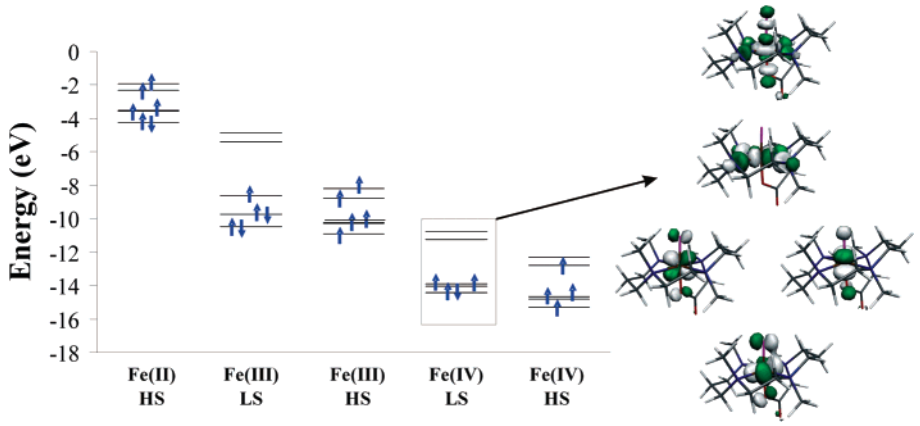

Figure 10. Energies of the 3d orbitals and electron configurations as a function of oxidation state and spin state calculated for the [(Me$_3$cyclam−acetate)-FeF]$^{n+}$ species (left). Contour plots of the valence 3d orbitals calculated from [(Me$_3$cyclam−acetate)FeF]$^{2+}$ showing their interactions with various ligand orbitals are shown to the right.

Plots of the iron 3d orbitals from [(Me$_3$cyclam−acetate)-FeF]$^{2+}$ are also shown in Figure 10, where it is clearly seen that they all have significant interactions with the orbitals of the ligands. There is a small but significant interaction of the d_{xy} orbital with *p* orbitals of the two axial ligands, which causes a tilting of the d_{xy} orbital slightly out of the N_4 plane. More significant are the antibonding π interactions between the axial ligands and the d_{xz} and d_{yz} orbitals, which cause significant energy difference (~4000 cm^{-1}) between the d_{xy} orbital and the nearly degenerate d_{xz}, d_{yz} set. The $d_{x^2-y^2}$ orbital interacts with sigma orbitals of the four equatorial nitrogen atoms, and the d_{z^2} orbital interacts with sigma orbitals of all of the ligand atoms and is therefore highest in energy.

DFT was also used to calculate spectroscopic properties of the three members of the electron-transfer series [(Me$_3$cyclam−acetate)FeF]$^{0/+/2+}$ for comparison with experiment to show convincingly that all of the redox reactions are metal based and that **2ox** indeed represents a genuine example of an octahedral Fe(IV) complex. These properties are summarized in Table 6 and compared to experimental values. It should be noted that the calculated properties of **2** have already been reported and discussed, and are shown here to facilitate comparison with the properties of **2red** and **2ox**.

The trend in the C═O stretching frequencies of the [(Me$_3$-cyclam−acetate)FeF]$^{n+}$ series is remarkably well reproduced by the calculations, though it should be noted that all of the calculated C═O stretching frequencies are uniformly 20−30 cm^{-1} higher than the experimental values. The C═O stretching frequencies correlate linearly with the calculated Fe−O distance to the bound carboxylate arm, and this correlation is shown in Figure 11 for the set of both calculated and experimental C═O stretching frequencies. Also shown is the calculated C═O stretch for an Fe(IV)-oxo species, [(Me$_3$cyclam−acetate)FeO]$^{2+}$ (vide infra) which also fits into this correlation very well. It appears that this correlation is electrostatic in origin and can be explained simply that as the Fe−O bond becomes stronger, the O−C═O acetate group has less π delocalization and therefore the C═O bond is more like a true double bond. This is also reflected in the C═O bond orders calculated from Löwdin analysis of (Me$_3$-cyclam−acetate)FeF, [(Me$_3$cyclam−acetate)FeF]$^{+}$, and [(Me$_3$-cyclam−acetate)FeF]$^{2+}$, which increase from 2.11 to 2.21 to 2.29.

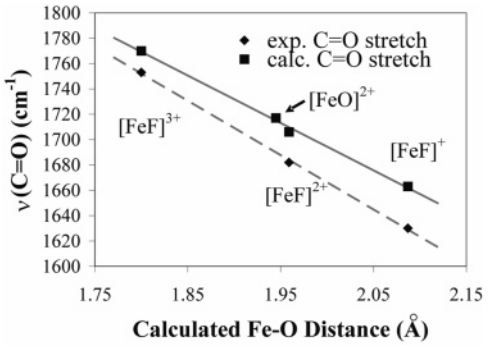

Figure 11. Plot of the C═O stretching frequencies of [(Me$_3$cyclam−acetate)FeF]$^{n+}$, n = 0,1,2, as well as [(Me$_3$cyclam−acetate)FeO]$^{+}$ against the calculated Fe−O bond distances between the iron ion and the carboxylate oxygen atom in each species. Both experimental and calculated C═O stretching frequencies are given, and the solid and dashed lines represent the results of linear least-squares fits.

Calculation of *g* and *D* tensors was also performed to compare with the experimental data for **2**, **2red**, and **2ox**. In general, good agreement between calculated and experimental values is observed. In particular, it should be noted that the negative sign of the *D* for **2red**, which is unusual because high-spin ferrous porphyrin species such as reduced cytochrome P450 and hemoglobin have positive *D* values,[49] is also suggested by the calculation. The calculated *D* value of [(Me$_3$cyclam−acetate)-FeF]$^{2+}$ is also in reasonable agreement with the value obtained for **2ox**, since the sign is correct though the calculated value is too low, due to reasons discussed more thoroughly elsewhere.[48] Both **2ox** and **3ox** have relatively large *D* values (>20 cm^{-1}), which appears to be a hallmark of S = 1 Fe(IV) species as similar results have been found in various ferryl complexes as well as an Fe(IV) complex synthesized by the Collins group having a macrocyclic equatorial ligand and two axial isonitrile ligands.[50] The large *D* values in these species have been attributed to spin orbit coupling of excited states, and in particular the low-lying S = 2 excited-state into the ground state.[48]

Mössbauer parameters and hyperfine coupling tensors may also be calculated using DFT with good accuracy.[51,52] The

(49) Debrunner, P. G. In *Iron Porphyrins Part III*; Lever, A. B. P., Gray, H. B., Eds.; VCH: Weinheim, 1989; Vol. III, pp 137.
(50) Collins, T. J.; Fox, B. G.; Hu, Z. G.; Kostka, K. L.; Münck, E.; Rickard, C. E. F.; Wright, L. J. *J. Am. Chem. Soc.* **1992**, *114*, 8724.
(51) Neese, F. *Inorg. Chim. Acta.* **2002**, *337*, 181.

Table 7. Calculated Properties[a] of [(Me_3cyclam−Acetate)FeO]$^+$

	$S=1$	$S=2$
Fe═O, Å	1.666	1.663
Fe−N_{av}, Å	2.103	2.200
Fe−O, Å	1.945	1.933
O−Fe−F, deg	176.0	175.1
Δd(Fe−N_4), Å	0.085	0.121
E, rel., kJ mol^{-1}	0	+11
Fe 3d spin density	1.34	3.13
Löwdin Fe═O bond order	1.5491	1.5622
ν(C═O), cm^{-1}	1717	1713
g_{iso}	2.018	2.013
D, cm^{-1}, E/D	+5.15, 0.007	+6.975, 0.01
δ, mm s^{-1}	0.128	0.18
ΔE_Q, mm s^{-1}, η	−0.243, 0.623	−1.587, 0.111
A, MHz	{−4.07, −29.80, −31.25}	{−24.63, −26.45, −42.06}

[a] Geometries were calculated using BP86/TZVP. Geometries using SV(P) are given in Table S2.

Table 8. Mössbauer and Spin Hamiltonian Parameters for $(FeO)^{2+}$ Species[a]

	[(cyclam–acetate)FeO]OTf	[(TPA)FeO(X)]$^{2+}$	[(Me_4cyclam)FeO($NCCH_3$)](OTf)$_2$	[(TMCS)FeO]$^+$	[(BPMCN)-FeO(NCR)]$^{2+}$	[$(H_2O)_5$FeO]$^{2+}$
$2S+1$	3	3	3	3	3	5
D, cm^{-1}, E/D	+23, 0	+28, 0	+28, 0	+35, 0	+19, 0.15	+9.7, −[b]
δ, mm s^{-1}	0.01	0.01	0.17	0.19	0.10	0.38
ΔE_Q, mm s^{-1}, η	1.37, 0.8	0.92, 0.9	+1.24, 0.5	−0.22, 0	1.75, 0.8	−0.33, 0
A_{xx}, A_{yy}, A_{zz}, MHz	−32, −32, −14	−32.4, −32.4, −6.9	−34, −28, −4	−23, −22, −5	−30, −23, −2	−[b], −28, −28
reference	18	27	23	28	27	16,17

[a] Structures for abbreviated ligands are given in the references. [b] Value not determined.

calculated isomer shifts and quadrupole splittings of the [(Me_3cyclam−acetate)FeF]$^{n+}$ series agree well with the values obtained experimentally for **2**, **2red**, and **2ox**. In particular, the change in sign of ΔE_Q for the Fe(III) species is well reproduced as has been previously mentioned.[25] Hyperfine constants describing the interaction of the unpaired spin with the ^{57}Fe nuclear spin have also been calculated, though it should be mentioned that the experimental values for **2red** and **2ox** are not very well defined, and therefore quantitative comparison is not appropriate. Qualitatively speaking, however, the basic pattern of the A values calculated for [(Me_3cyclam−acetate)-FeF]$^{2+}$ (all three A values being negative, one small and two large and nearly equal) is similar to what has been observed for ferryl species, as well as in **3ox**, where the A values are more well defined.

Spectroscopic properties were also calculated for the hypothetical high-spin [(Me_3cyclam−acetate)FeF]$^{2+}$ dication ($S=2$) to compare with what is known for the low-spin Fe(IV) species. The C═O stretch, g value, and isomer shift are not very different from what is calculated for the low-spin species, but the calculated D value of 10.3 cm^{-1} for the high-spin species is nearly twice as large as that of the low-spin species and is rhombic rather than axial. Although this D value is significantly larger than that reported for the five-coordinate high-spin Fe(IV) complex of Collins (−3.7 cm^{-1}),[53] it agrees well with the D value reported for the ferryl aquo ion [$(H_2O)_5$FeO]$^{2+}$ (+9.7 cm^{-1}).[16,17] One major difference between high- and low-spin [(Me_3cyclam−acetate)FeF]$^{2+}$ is that the calculated quadrupole splitting of +0.47 mm s^{-1} for the high-spin species is much smaller than the calculated value for the low-spin species (+2.31 mm s^{-1}) and from the observed value (+2.43 mm s^{-1}). This observation further supports our assignment of **2ox** as being a low-spin Fe(IV) complex rather than being high-spin.

Fe(IV)-Fluoro vs Fe(IV)-Oxo: Isoelectronic Cousins. We may consider the $(FeF)^{3+}$ moiety to be isoelectronic to $(FeO)^{2+}$. Because there is now a considerable wealth of spectroscopic and structural data for Fe(IV)-oxo species due to recent synthetic breakthroughs in the Que lab,[23] it is pertinent to compare the electronic structure and properties of [(Me_3cyclam−acetate)-FeF]$^{2+}$ with those of the corresponding oxo complex, [(Me_3-cyclam−acetate)FeO]$^+$, which may be considered as an analog of the complex [(cyclam−acetate)FeO]OTf which was previously reported in our group.[18] Geometric and spectroscopic properties of the hypothetical cation [(Me_3cyclam−acetate)-FeO]$^+$ have been calculated and are presented in Table 7 and shall be here compared to the properties of known $(FeO)^{2+}$ species which have been collected in Table 8.

The calculated geometry of [(Me_3cyclam−acetate)FeO]$^+$ is in good agreement with the known structural data on FeO^{2+} species; in particular the Fe═O bond distance of 1.67 Å is very close to that observed in the crystal structure of [(Me_4cyclam)-FeO($NCCH_3$)](OTf)$_2$, 1.65 Å. This distance is interestingly shorter than the calculated Fe−F distance for **2ox** by ∼0.1 Å, emphasizing the difference in bond orders for the two species. The calculated Fe═O bond order, 1.55, is considerably greater than the Fe−F bond order, 0.86, clearly reflecting more π bonding in the ferryl species. The Fe−O bond to the acetate arm in the ferryl complex is elongated by 0.15 Å as compared to the Fe(IV)-fluoro species, reflecting the greater trans influence of the short Fe═O multiple bond.

As seen in Table 8, a large positive zero-field splitting value (>10 cm^{-1}) is typical of ferryl species. Indeed, all of the non-oxo Fe(IV) species presented here share this characteristic, and this is reproduced in the calculation of both the Fe(IV)-fluoro and −oxo species to the same degree of accuracy. In both

(52) Sinnecker, S.; Slep, L. D.; Bill, E.; Neese, F. *Inorg. Chem.* **2005**, *44*, 2245.
(53) Kostka, K. L.; Fox, B. G.; Hendrich, M. P.; Collins, T. J.; Rickard, C. E. F.; Wright, L. J.; Münck, E. *J. Am. Chem. Soc.* **1993**, *115*, 6746.

species, an axial D of $\sim+5$ cm^{-1} is calculated, which is a surprising result because theoretical analysis of zero-field splittings in ferryl species reveals that the triplet-quintet energy gap is one of the major factors contributing to the large D value. In the case of the FeF^{3+} species, however, this energy difference (50 kJ mol^{-1}) is computed to be much larger than in the case of the FeO^{2+} species (11 kJ mol^{-1}) which should lead to a D value in the former ion which is much smaller than in the ferryl species. We suggest that the unusually large D value for the fluoro complex is due to the fact that the covalency of the Fe−F bond is much lower than that of the Fe═O bond, which allows more efficient spin−orbit coupling contributions to the D value. The hyperfine tensor values are also similar for both FeF^{3+} and FeO^{2+} species because for both the Fe(IV)-fluoro and −oxo species, A values of $A_{11} \ll A_{22} \approx A_{33}$ are calculated and this pattern fits well the experimental examples (Table 6 and 8).

From the survey of Mössbauer parameters of low-spin ferryl species (Table 8), the quadrupole splittings can vary over a wide range (from −0.22 to +1.24 mm s^{-1}, though often the sign is not well defined because of the large asymmetry parameter η) whereas the isomer shifts generally are limited to the range of 0.01 to 0.19 mm s^{-1}. Thus, the quadrupole splitting parameter is apparently very sensitive to the coordination sphere of the molecules, but not in a readily predictable way. This contrasts with the octahedral non-oxo Fe(IV) species presented here where a large positive ΔE_Q value is observed. Because in both oxo- and non-oxo species the $(d_{xy})^2(d_{xz})^1(d_{yz})^1$ configuration leads to the same valence contribution to the electric field gradient (EFG) tensor (which should lead to a ΔE_Q value that is large and positive), the effect of the more covalent Fe═O double bond is to decrease the ΔE_Q value significantly.

In fact, it is unfair to assign the $(d_{xy})^2(d_{xz})^1(d_{yz})^1$ configuration to Fe(IV)-oxo species because the d_{xz} and d_{yz} orbitals form strong covalent π bonds to p orbitals of the oxygen atom. The singly occupied orbitals in ferryl species are essentially Fe−O π^* orbitals having 60.3% Fe 3d character and 34.8% O p character and these are raised in energy by $\sim$15 000 cm^{-1} above the doubly occupied d_{xy} orbital, similar to what has been found from DFT analysis of $[(Me_4cyclam)FeO]^{2+}$.[54] This large splitting within the t_{2g} level (which we shall call Π) is not nearly as large in **2ox**, in which a splitting of only 4,500 cm^{-1} between the d_{xy} and d_{xz}, d_{yz} occurs. This result agrees well with the differences in the electronic spectra of **2ox** and typical ferryl species. The latter species typically have a number of bands with $\epsilon < 500$ M^{-1} cm^{-1} in the region from 500 to 1100 nm, whereas this region in the spectrum of **2ox** is empty. These bands for the ferryl species have been assigned as d → d transitions,[54] arising in the visible to near IR range due to the large value of Π. In **2ox**, the corresponding bands will be much higher in energy due to both the smaller value of Π and the value of 10Dq of around 30 000 cm^{-1} and would undoubtedly be masked by the very intense charge-transfer bands from 350−450 nm.

The high-spin ($S = 2$) state of $[(Me_3cyclam-acetate)FeO]^+$ was also calculated and was found to be only 11 kJ mol^{-1} higher in energy than the $S = 1$ ground state, which is a remarkable difference to the case of $[(Me_4cyclam)FeO]^{2+}$, in which the high-spin state was calculated to be 54 kJ mol^{-1} in energy above the $S = 1$ state.[54] This is also remarkably smaller than the calculated energy difference between low- and high-spin **2ox** (50 kJ mol^{-1}) and is so small that the $S = 1$ and $S = 2$ states of this complex should be considered to be very close in energy. We currently plan to synthesize the complex to determine the nature of the ground state experimentally.

(54) Decker, A.; Rohde, J. U.; Que, L., Jr.; Solomon, E. I. *J. Am. Chem. Soc.* **2004**, *126*, 5378.

Conclusions

A new family of non-oxo Fe(IV) complexes is presented and characterized by spectroelectrochemistry, Mössbauer spectroscopy, and DFT calculations. The calculated and spectroscopically observed changes in **1**, **2**, and **3** upon oxidation and reduction are consistent with the presence of iron-centered redox processes. This gives us a unique opportunity to observe Fe(II), Fe(III), and Fe(IV) complexes with essentially the same ligand sphere. In all cases, the complexes become more highly colored as the oxidation state of the iron increases, as is expected due to the shortening of the metal−ligand bond distances (and hence the lowering in energy of LMCT bands in the electronic spectrum). For the series **2red**/**2**/**2ox**, the calculated structures indicate a contraction of *all* of the iron-ligand bond distances upon increasing oxidation number, and a $(d_{xy})^2(d_{xz})^1(d_{yz})^1$ ground state configuration is found for **2ox**. The Fe(IV)-oxo species $[(Me_3cyclam-acetate)FeO]^+$ is isoelectronic to the cation of **2ox** but is different from the fluoro complex in many ways, all of which are related to the increased covalency of the Fe═O double bond in the ferryl species. This strong covalent bond affects the Fe(IV) center by elongating the iron-ligand bond *trans* to the Fe═O bond, slightly increasing the isomer shift, significantly decreasing the quadrupole splitting, and increasing the separation between the d_{xy} orbital and the d_{xz} and d_{yz} (which are strongly π antibonding with respect to the oxygen atom). The last effect causes weak electronic transitions to appear in the absorption spectrum of ferryl species in the range from 500 to 1100 nm, which are absent in the case of **2ox**.

Experimental

General. The complex $(Me_3cyclam-acetate)Fe-O-FeCl_3$ was prepared according to the previously reported procedure.[25] $[(Me_3cyclam-acetate)FeF]PF_6$ can be prepared from $(Me_3cyclam-acetate)Fe-O-FeCl_3$ as previously reported,[25] but we also report here a new method below that leads to better purity. All solvents and reagents were used as received.

$[(Me_3cyclam-acetate)FeCl]PF_6$ (1). Solid $(Me_3cyclam-acetate)Fe-O-FeCl_3$ (0.100 g, 0.188 mmol) was mixed with a solution of KPF_6 (0.208 g, 1.13 mmol) in 5 mL of water for 14 h, causing the slow precipitation of a bright-yellow powder. This was collected by filtration and dried in air to yield 61 mg (61%) of the product. IR (KBr, cm^{-1}): 3454 m, br, 2906 w, 1682 s (C═O), 1456 m, 1340 w, 1297 m, 1105, w, 1089 w, 996 w, 955 m, 923 w, 839 vs (PF_6), 744 w, 714 w, 557 s. ESI+ mass spectrum (m/z, amu): 390 $(M-PF_6)^+$, 355.3 $(M-PF_6-Cl)^+$. Anal. calcd for $C_{15}H_{31}N_4FeClPF_6$: C 33.63, H 5.83, N 10.46%. Found: C 34.25, H 5.75, N 10.24%.

$[(Me_3cyclam-acetate)FeF]PF_6$ (2). A solution of $[(Me_3cyclam-acetate)FeCl]PF_6$ (0.056 g, 0.105 mmol) in 20 mL of water was heated gently to 80° for a few minutes during which time a light-orange precipitate (rust) was observed. The mixture was filtered to give a brilliant-yellow solution, which was concentrated and allowed to evaporate slowly in air. After 1 week, large crystals of the fluoro complex had grown, which were collected and washed with Et_2O. Yield: 20 mg, 37%. Complete evaporation of the solution yields a messy mixture. IR (KBr, cm^{-1}): 3455 w, br, 2969, w, 1682 s (C═O), 1470 m, 1338 w, 1298 s, 1262 w, 1154 w, 1107 w, 1092 w, 1059 w,

1023 w, 969 w, 918 w, 841 vs (PF_6), 822 s, 746 w, 712 w, 558 s, 543 m. ESI+ mass spectrm (*m*/*z*, amu): 374 $(M-PF_6)^+$. Anal. calcd for $C_{15}H_{31}O_2N_4FePF_7$: C 34.70, H 6.02, N 10.79%. Found: C 34.80, H 6.10, N 10.58%.

[(Me$_3$cyclam−acetate)FeN$_3$]PF$_6$ (3). To a mixture of Me$_3$cyclam−acetateFe−O−$FeCl_3$ (0.300 g, 0.563 mmol) and 1.5 mL of MeOH was added solid NaN_3 (0.366 g, 5.63 mmol), resulting in a deep-red mixture, to which a solution of KPF_6 (0.622 g, 3.38 mmol) in 15 mL of water was added. The resulting red mixture was stirred in the dark for 14 h, resulting in a red solid and red supernatant solution. The solid was collected by filtration, washed with Et_2O, dried, and extracted with acetonitrile to give a brilliant red-orange solution. This was allowed to evaporate slowly in the dark to yield a crop of large red crystals, which were collected, washed with EtOH and Et_2O, and dried in air. Yield: 175 mg, 57%. The compound is somewhat light sensitive in solution. IR (KBr, cm^{-1}): 3432 s, br, 2090 vs (N_3), 1671 s (C═O), 1465 m, 1367 m, 1296 m, 1023 w, 968 w, 956 w, 916 w, 844 s (PF_6), 744 w, 558 m. ESI+ mass spectrum (*m*/*z*, amu): 397.2 $(M-PF_6)^+$. Anal. calcd for $C_{15}H_{31}O_2N_7FePF_6$: C 33.22, H 5.76, N 18.08%. Found: C 33.10, H 5.23, N 17.24%.

[NEt$_4$][^{57}FeCl$_4$]. A sample of ^{57}Fe foil (32 mg, 0.56 mmol) was dissolved in hot concentrated HCl (over Pt foil, to expedite the process). The resulting yellow solution was cooled to room temperature, and the solvent was removed in a rotary evaporator yielding an orange solid residue. This was dissolved in a minimal amount of EtOH (∼1 mL), and added to a solution of excess NEt_4Cl, which was also dissolved in a minimal amount of EtOH (∼1 mL). Upon mixing, a soft-yellow precipitate appeared, and the mixture was stirred for ∼30 min to ensure complete reaction. The solid was collected by filtration, washed with Et_2O, and dried in air. Yield: 154 mg, 83%. Isotopically enriched compounds were prepared using a 40:60 ratio of $[NEt_4][^{57}FeCl_4]$ and normal $[NEt_4][FeCl_4]$. ($[NEt_4][FeCl_4]$ is the starting material used to synthesize (Me$_3$cyclam−acetate)Fe−O−$FeCl_3$.)

Physical Measurements. IR spectra were recorded in the range 400−4000 cm^{-1} on a Perkin-Elmer 2000 FT-IR spectrometer on samples pressed into KBr discs. ESI mass spectra were obtained on a Finnigan MAT 95 spectrometer. Elemental analyses were done by the H. Kolbe Mikroanalytisches Laboratorium in Mülheim an der Ruhr, Germany. Variable temperature magnetic susceptibilities were measured on a Quantum Design SQUID magnetometer in the range 2−300 K at an applied external field of 1000 G. Data points were corrected for intrinsic diamagnetism of the sample, the sample holder, and also for temperature-independent paramagnetism. X-Band EPR spectra were recorded at 10 K on a Bruker ESP 300E spectrometer equipped with a helium-flow cryostat (Oxford Instruments ESR 910). Mössbauer spectra were recorded on an alternating constant-acceleration spectrometer with a minimum line width of 0.24 mm s^{-1}. The sample temperature was maintained by an Oxford Instruments Variox cryostat for zero-field measurements, or by an Oxford Instruments Mössbauer-Spectromag 2000 cryostat, which was used for measurements in applied magnetic fields with the field oriented perpendicular to the γ source. Isomer shifts (δ) are referenced against iron metal at 300 K.

Computations. The species (Me$_3$cyclam−acetate)FeF ($S = 2$), $[$(Me$_3$cyclam−acetate)FeF$]^+$ ($S = {}^1/_2$ and $S = {}^5/_2$, data previously reported[25]), $[$(Me$_3$cyclam−acetate)FeF$]^{2+}$ ($S = 1, 2$), and $[$(Me$_3$cyclam−acetate)FeO$]^+$ ($S = 1, 2$) were used as models for density functional theory calculations, which were performed using the ORCA program package.[55] The initial geometry of $[$(Me$_3$cyclam−acetate)FeF$]^+$ ($S = {}^5/_2$) was taken from its crystal structure as described previously[25] and optimized using the BP86 functional and using the SV(P) and TZVP basis sets.[56,57] These optimized geometries were used as starting geometries for (Me$_3$cyclam−acetate)FeF and $[$(Me$_3$cyclam−acetate)-FeF$]^{2+}$ ($S = 1, 2$), whose geometries were optimized in the same way. The optimized geometries of $[$(Me$_3$cyclam−acetate)FeF$]^{2+}$ were used as starting geometries for the geometry optimization of $[$(Me$_3$cyclam−acetate)FeO$]^+$. For all structures, the triple-ζ optimized geometries were used for calculations of the total energy and all properties. Vibrational frequencies were calculated using the BP86 functional using a numerical differentiation of analytic gradients with an increment of 0.005 Bohr. In the high-spin $[$(Me$_3$cyclam−acetate)FeF$]^{2+}$ dication, a negative vibrational frequency of -9 cm^{-1} was observed, but the geometry was not reoptimized because the frequency is small and does not correspond to an important vibrational mode of the molecule and since the calculated molecule is a hypothetical one. In all other cases, no negative frequencies were observed, indicating that the structures correspond to potential energy minima. Zero-point vibrational energies and thermal corrections were taken from these frequency calculations. Total energies were calculated with the B3LYP functional. Mössbauer parameters (including magnetic hyperfine tensors) were calculated at the B3LYP level using the triple-ζ basis set and an expanded CP(PPP) basis set[51] for iron, as described previously.[51] The *g* tensors and *D* tensors were calculated according to previously developed procedures.[48,58−60] Orbitals were visualized using the Molekel program.[61]

Acknowledgment. We thank the Fonds der Chemischen Industrie for financial support. J.F.B. thanks the Alexander von Humboldt Foundation for a postdoctoral fellowship.

Supporting Information Available: Tables S1 and S2; Figures S1−S4. This material is available free of charge via the Internet at http://pubs.acs.org.

JA063590V

(55) Neese, F. *ORCA - an ab initio, DFT, and Semiempirical Electronic Structure Package*, 2.4, revision 29; Max-Planck-Institut für Strahlenchemie: Mülheim, Germany, **2003**.
(56) Schafer, A.; Horn, H.; Ahlrichs, R. *J. Chem. Phys.* **1992**, *97*, 2571.
(57) Schafer, A.; Huber, C.; Ahlrichs, R. *J. Chem. Phys.* **1994**, *100*, 5829.
(58) Neese, F. *J. Chem. Phys.* **2001**, *115*, 11080.
(59) Neese, F.; Solomon, E. I. *Inorg. Chem.* **1998**, *37*, 6568.
(60) Ray, K.; Begum, A.; Weyhermüller, T.; Piligkos, S.; van Slageren, J.; Neese, F.; Wieghardt, K. *J. Am. Chem. Soc.* **2005**, *127*, 4403.
(61) Flükiger, P.; Lüthi, H. P.; Portmann, S.; Weber, J. *MOLEKEL 4.0*; Swiss Center for Scientific Computing: Manno, Swizerland, 2000.